Time-Resolved Observation of Ultrahigh Intensity Laser-Produced Electron Jets Propagating through Transparent Solid Targets

L. Gremillet,[1] F. Amiranoff,[1] S. D. Baton,[1] J.-C. Gauthier,[1] M. Koenig,[1] E. Martinolli,[1] F. Pisani,[1] G. Bonnaud,[2] C. Lebourg,[2] C. Rousseaux,[2] C. Toupin,[2] A. Antonicci,[3] D. Batani,[3] A. Bernardinello,[3] T. Hall,[4] D. Scott,[4] P. Norreys,[5] H. Bandulet,[6] and H. Pépin[6]

[1]*Laboratoire pour l'Utilisation des Lasers Intenses, UMR7605, CNRS-CEA-Université Paris VI-Ecole polytechnique, 91128 Palaiseau, France*

[2]*Commissariat à l'Énergie Atomique, 91680 Bruyères-le-Châtel, France*

[3]*Dipartimento di Fisica G. Ochiolini, Universita degli Studi di Milano-Bicocca and INFM, Via Emanueli 15, 20126 Milan, Italy*

[4]*Department of Physics, University of Essex, Colchester CO4 3SQ, United Kingdom*

[5]*Rutherford Appleton Laboratory, Chilton, Didcot, Oxon OX11 OQX, United Kingdom*

[6]*INRS-Énergie et Matériaux, J3X1S2 Varennes, Québec, Canada*

(Received 16 July 1999)

We report on shadowgraphic measurements showing the first space- and time-resolved snapshots of ultraintense laser pulse-generated fast electrons propagating through a solid target. A remarkable result is the formation of highly collimated jets (<20-μm) traveling at the velocity of light and extending up to 1 mm. This feature clearly indicates a magnetically assisted regime of electron transport, of critical interest for the fast ignitor scheme. Along with these jets, we detect a slower ($\approx c/2$) and broader (up to 1 mm) ionization front consistent with collisional hot electron energy transport.

PACS numbers: 52.35.–g, 52.40.–w, 52.60.+h

The fast ignitor scheme, which claims to relax some of the constraints hampering the standard approaches to inertial confinement fusion, has triggered a worldwide interest since its inception [1]. It hinges on the rapid additional heating of the core of a precompressed thermonuclear pellet due to the slowing down of a bunch of relativistic electrons generated by an ultraintense laser pulse. Now, the highly overcritical plasma surrounding the core should prevent any laser pulse from reaching it, whatever high-intensity penetration mechanisms are at work (relativistic self-induced transparency [2] or ponderomotive hole boring [3]). An encouraging point is that particle-in-cell simulations predict a rather peaked hot electron distribution in the vicinity of the laser-solid interaction zone [4]. However, an efficient heating of the core requires the electron beam to remain collimated up to its final absorption zone, i.e., on a distance of several hundreds of microns. This can be achieved only through the pinching effect of the beam-driven magnetic field competing with multiple scattering. Therefore, fast electron transport from moderately to extremely dense regions appears as a key issue for the success of fast ignition, which must be thoroughly tackled both experimentally and theoretically.

Over the past year, there has been a growing body of experimental evidence pointing to the existence of very collimated high intensity laser-produced electron jets traveling through solid targets. Tatarakis *et al.* have recently observed a narrow expanding plasma at the rear surface of thick plastic slabs irradiated by a 1 ps, 10^{19} W/cm^2 laser pulse [5]. By using a 2D Fokker-Planck hybrid code, they interpreted this localized rear heating as a magnetic field-enhanced electron energy deposition at the target/vacuum interface [6]. This effect has also been detected in other experiments [7]. Though very encouraging, these studies still provide an incomplete experimental picture of the phenomena arising in the bulk of the target.

In the present paper, we report on optical shadowgraphic results showing what is, to our knowledge, the first comprehensive set of space- and time-resolved snapshots of fast electrons propagating through a solid target. In order to bypass the classical limitation of optical probing into an overcritical solid target, we use transparent glass slides. Our measurements pinpoint the existence of two types of fast electron propagation occurring simultaneously. First, a filament-shaped structure is clearly evidenced on a several hundred-micron scale length. As has been stressed above, this is the long-awaited confirmation of a feature particularly critical for the fast ignition. Along with this collimated jet, a more standard collisional propagation is seen to take place. The purpose of this paper is to set the experimental basis for a numerical modeling that will be developed in a future publication.

The experiment was performed with the new LULI 100 TW laser based on chirped pulse amplification. A 350 fs, 0.53-μm laser pulse with an energy up to 10 J was focused by a $f/3$ off-axis parabola at normal incidence onto the 500-μm-wide edge of a fused silica plate as shown in Fig. 1. Low-energy equivalent-plane measurements showed a 4-μm full width at half maximum (FWHM) focal spot. Pinhole imaging of the x-ray emission (<1.5 keV) monitored the focal spot size for each full-energy shot. With a 5-μm aperture and a 40-μm

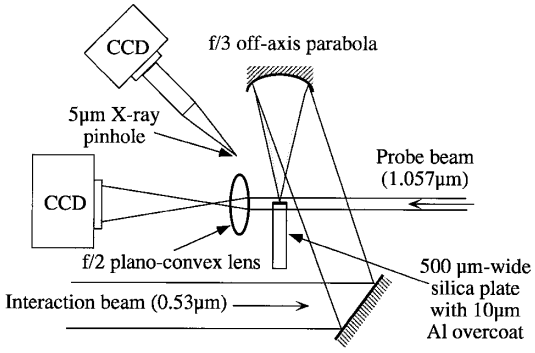

FIG. 1. Experimental setup.

Al filter, an average 8-μm FWHM focal spot was obtained. From K_α measurements on multilayered targets performed during the same experimental runs and showing an average hot electron temperature of 400 keV, we can estimate an incident laser intensity of the order of 10^{19} W/cm^2 [8]. The regime considered here is therefore moderately relativistic.

In order to cope with the sensitivity of the silica plate to any prepulse that might either propagate unaltered if below the damage threshold or create a plasma that one might wrongly construe as a fast electron-induced ionization, each target was coated with a 10-μm Al foil. This is enough to prevent any transmission of the laser light. Moreover, frequency doubling of the laser beam allows a contrast ratio better than 10^{10}:1 in the frequency doubled beam. The use of four dichroic mirrors located between the potassium dihydrogen phosphate crystal and the target decreases the level of a nonconverted 1.057-μm pulse by a factor of 10^8.

A probe beam uses a small energy fraction of the nonconverted interaction beam. After compression, this short pulse allows a 2D transverse imaging of the backlit target on a 1.057-μm-filtered charge coupled device (CCD) detector, with spatial and time resolutions, respectively, of the order of 5 μm and 600 fs. The region that has been ionized up to a fraction of the critical density of 1.057-μm light becomes opaque to the probe. By varying the time delay between the probe and the main beam, we are able to analyze the ionization dynamics occurring within the glass slab. The very high contrast of the interaction beam was confirmed by the lack of any preplasma absorption for negative time delays between the probe and the main pulse.

The shadowgraphic images of the target at three successive times are presented in Fig. 2. The first picture (see Fig. 2a) is taken 1.2 ps after the interaction pulse. In order to enhance the contrast of this particular image, we subtracted from it the image of the unperturbed target in the presence of the probe beam alone. Thus, we can clearly see two narrow ($\approx$20-μm), 350-μm-long jets originating from the focal spot. Their length corresponds to a velocity very close to the velocity of light. Also visible, if less surprising, is the shape of a roughly isotropic cloud centered on the focal spot, and extending up to 180 μm. This feature becomes even more conspicuous on the two following images recorded, respectively, at 2.2 and 3 ps. The extent of the cloud front is plotted as a function of time in Fig. 3. By fitting a line to this plot, we infer an expansion velocity of the order of 1.6×10^{10} cm/s. This velocity exceeds by more than 1 order of magnitude the velocities characterizing electron thermal conduction [9] or radiation driven thermal transport, as has been recently reported with a similar diagnostic but at lower intensities [10].

Given the 10-μm Al coating and the high contrast ratio of the laser pulse, we can arguably rule out the presence of any laser light within the target and thus assume that the only processes to be looked upon are due to fast electrons or hard x rays. The latter may be split up into two groups: the thermal emission at the target Al surface due to the laser heating itself and the discrete (mostly K_α) and continuous (bremsstrahlung) x-ray generation by the fast electrons either in the Al foil or the silica slide. The 1D hydro code MULTI [11] was used to model the transport of the laser-generated photons. The MULTI simulations reproduced

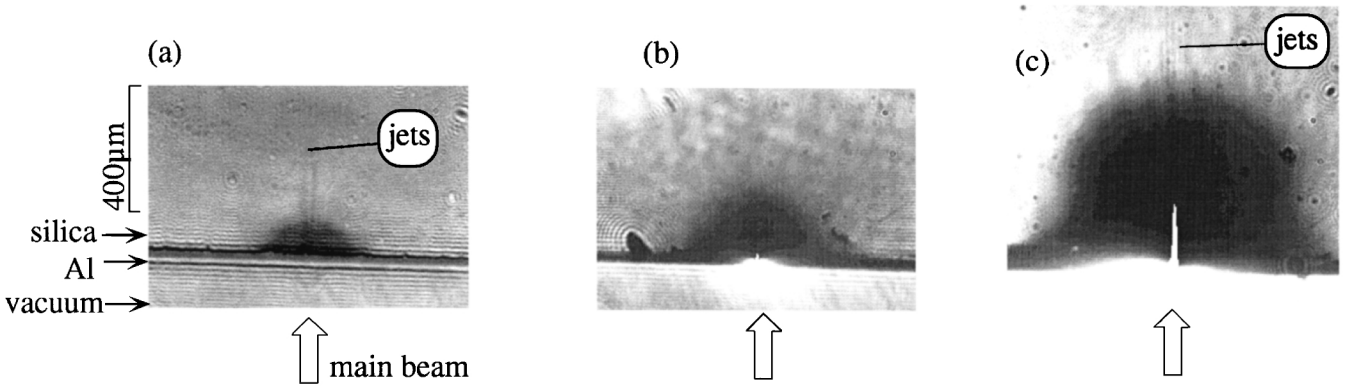

FIG. 2. Shadowgraphic images of the silica target at three times, (a) 1.2 ps, (b) 2.2 ps, and (c) 3 ps after the interaction pulse. Note that in (a) the fringes inside the cloud are an artifact of the image subtraction process (the diffraction pattern at the target edge being present only in the reference image).

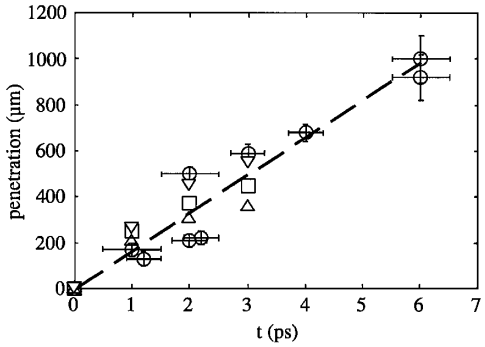

FIG. 3. Cloud front penetration as a function of time: measured values (circles), linear fit of the experimental values (dashed line), simulation with 1 J total energy and 200 keV Maxwellian temperature (down triangles), with 100 keV Maxwellian temperature (squares), and with 70 keV Maxwellian temperature (up triangles).

the measured ionization front velocity over the first two picoseconds. Yet, the radiative scenario was dismissed by a series of shots on targets comprising a 200-μm vacuum gap that allowed the regions of generation and transport of the electrons to be separated. We found that the presence of vacuum dramatically affects the energy transport into silica, as exhibited in Fig. 4. These two images were recorded 6 ps after the interaction beam: on the left, that is, with the standard Al/SiO_2 target, a large ($\approx$1 mm) cloud is seen, as well as many jets. On the right, that is, with the 200-μm vacuum gap, we cannot see any ionized structure into the transparent region. This demonstrates, first, that the bulk of the electrons are stopped in vacuum owing to space-charge or magnetic field effects, and, second, that the ionized features are not of radiative nature, the vacuum gap being no obstacle for the x rays.

We modeled the cloud propagation using a new 3D electron transport code (PÂRIS) whose development is currently under way [12]. Derived from the hybrid scheme presented by Davies *et al.* [13], it aims at modeling both the

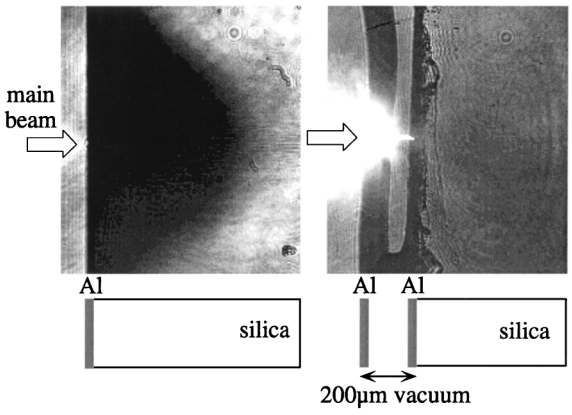

FIG. 4. Shadowgraphic images taken 6 ps after interaction of the main pulse with (left) a standard target and (right) a target comprising a 200-μm vacuum gap.

effects of collisions (i.e., multiple scattering and slowing down) and self-generated magnetic fields. The very shape of the cloud suggests a mainly collisional regime of propagation, which is supported by PÂRIS simulations where we switched off the electromagnetic fields. The energy loss due to the free and bound electrons of the plasma is calculated over each time step in the continuous deceleration approximation according to the Bethe-Bloch cross section [14]. The contribution of the excitation of the plasma oscillations is accounted for by means of the Pines-Bohm formula [15]. The multiple scattering is described using the Moliere distribution [16]. To estimate the temperature increase and the ionization rate into silica, we took advantage of the scaling laws given by Vu *et al.* [17]. As an input, 1D relativistic Maxwellian electron distributions, with a total energy of 1 J (inferred from the K_α measurements showing a 10% conversion efficiency of laser energy into fast electrons [18]) and a temperature varying from 70 to 200 keV, were injected over 300 fs into silica. Given a simulated temperature map (see Fig. 5) and Vu's formula, we performed ray-tracing calculations in the resulting inhomogeneous electronic density profile so as to determine the boundary of the region opaque to the probe beam and better the comparison with the experimental pictures. We found that it corresponds to the 0.2 eV frontier, indicated by the solid line in Fig. 5. As a result, the cloud penetration velocity was well reproduced by this purely collisional model, the best fit being obtained for a 200 keV hot temperature. For slightly later times that were still attainable with our simulations, the numerical results (see Fig. 3) seem to reach a plateau, contrary to the quite monotonous experimental trend. We attribute this discrepancy to the absence in our code of some mechanisms as electrical breakdown or the secondary electron generation which may ease the expansion of the ionized region.

The observation of filamented hot electron structures obviously points to the role of self-generated magnetic fields. It has long been known that the interplay of magnetic focusing and collisionless pressure effects may result in a self-guiding regime in tenuous plasmas [19]. In the case of solid-density targets, the first numerical predictions of such large-scale (up to 250-μm) collimated transport were obtained by Davies *et al.* [6,13], albeit they only considered preionized, and therefore low-resistivity, media. Indeed, we might expect an important suprathermal transport inhibition due to the initial insulator resistivity of silica. Fortunately, as shown in preliminary short-scale PÂRIS simulations in high-resistivity matter ($\eta \approx 10^{-2}\ \Omega\,\mathrm{m}$), the electrostatic field generated in the very first femtoseconds of the interaction reaches peak values far higher than the breakdown field in silica ($E_b \sim 10^8$ V/cm) [20]. Thus, the insulator resistivity of cold silica will rapidly not apply. Besides a fast decrease in the electrostatic inhibition, the insulator/plasma transition allows an important fast current neutralization by a cold return current. This process is particularly crucial for a stable magnetic

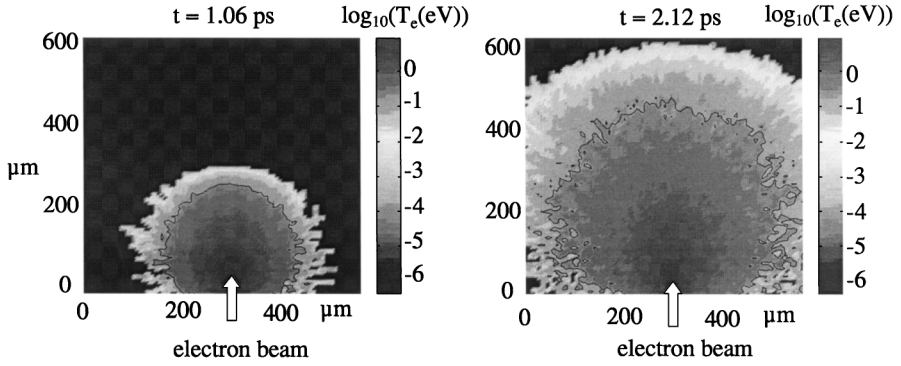

FIG. 5. Log_{10} of the simulated temperature increase in silica for a 1 J, 200 keV Maxwellian distribution of electrons emitted in 300 fs. Only collisional processes are taken into account. The solid line corresponds to the 0.2 eV boundary.

field-assisted regime, since the incident fast current largely exceeds the well-known Alfvén limit [21].

The presence of several jets may be attributed to different breakup instabilities taking place all along the hot beam's path. In the laser-heated zone, where the distinction between fast and return currents is somewhat blurred, the Weibel instability gives rise to a filamented pattern before subsequent coalescing of the trapping regions [4,22]. Deeper into the target, other instabilities due to the resistive medium response may then take place as filamentation [21], or Haines' electrothermal instability [23].

In summary, we experimentally confirmed the ability of relativistic laser-pulse-produced fast electrons to propagate over long distances into solid-density targets. Along with this dramatic feature, another regime of ultrafast energy transport, seemingly related to collisional electron propagation, has been observed. Among the fast ignitor-related issues that remain to be addressed is an explanation for this dual electron behavior and an assessment of the dominant process as regards the heating efficiency.

We gratefully acknowledge the support of the LULI laser staff and Mrs. Millérioux from CEA/Bruyères-le-Châtel for providing the targets. This work was supported by the E.U. TMR Laser Facility Access Program (Contract No. ERBFMGE-CT95-0044).

[1] M. Tabak *et al.*, Phys. Plasmas **1**, 1626 (1994).
[2] E. Lefebvre and G. Bonnaud, Phys. Rev. Lett. **74**, 2002 (1995); S. Guérin *et al.*, Phys. Plasmas **3**, 2693 (1996).
[3] S. C. Wilks *et al.*, Phys. Rev. Lett. **69**, 1383 (1992).
[4] A. Pukhov and J. Meyer-ter-Vehn, Phys. Rev. Lett. **79**, 2686 (1997).
[5] M. Tatarakis *et al.*, Phys. Rev. Lett. **81**, 999 (1998).
[6] J. R. Davies *et al.*, Phys. Rev. E **59**, 6032 (1999).
[7] J. Fuchs *et al.*, Phys. Plasmas **6**, 2569 (1999).
[8] F. N. Beg *et al.*, Phys. Plasmas **4**, 447 (1997).
[9] Y. B. ZelDovich and Y. P. Raizer, *Physics of Shock Waves and High-temperature Hydrodynamic Phenomena,* edited by W. D. Hayes and R. F. Probstein (Academic Press, New York, 1966).
[10] T. Ditmire *et al.*, Phys. Rev. Lett. **77**, 498 (1996); E. T. Gumbrell *et al.*, Phys. Plasmas **5**, 3714 (1998).
[11] R. Ramis *et al.*, Comput. Phys. Commun. **49**, 475 (1988).
[12] L. Gremillet *et al.*, Third International Workshop on the Fast Ignition of Fusion Targets, CLRC Report No. RAL-TR-1998-085, 1998 (unpublished).
[13] J. R. Davies *et al.*, Phys. Rev. E **56**, 7193 (1997).
[14] F. Rohrlich and B. C. Carlson, Phys. Rev. **93**, 38 (1954).
[15] D. Pines and D. Bohm, Phys. Rev. **85**, 338 (1952).
[16] H. Bethe, Phys. Rev. **89**, 1256 (1953).
[17] B. T. Vu *et al.*, Phys. Plasmas **2**, 476 (1995).
[18] F. Pisani *et al.*, Third International Workshop on the Fast Ignition of Fusion Targets, CLRC Report No. RAL-TR-1998-085, 1998 (unpublished).
[19] W. H. Bennett, Phys. Rev. **45**, 890 (1934).
[20] D. von der Linde and H. Schüler, J. Opt. Soc. Am. B **13**, 216 (1996).
[21] S. Humphries, *Charged Particle Beams* (Wiley Interscience, New York, 1990).
[22] R. L. Morse and W. C. Nielson, Phys. Fluids **14**, 830 (1971).
[23] M. G. Haines, Phys. Rev. Lett. **47**, 917 (1981).